JOURNAL OF MATERIALS SCIENCE 22 (1987) 925–931

# Ferroelectric domain configurations in a modified-PZT ceramic

C. A. RANDALL, D. J. BARBER
*Department of Physics, University of Essex, Wivenhoe Park, Colchester, Essex CO4 3SQ, UK*
R. W. WHATMORE
*Allen Clark Research Centre, Caswell, Towcester, Northants NN12 8EQ, UK*

Transmission electron microscopy and electron diffraction have been used to study ferroelectric domain configurations in a modified-PZT ferroelectric ceramic which has rhombohedral symmetry. Wedge-shaped domains with head-to-tail dipole arrangements and fine lamellar domains are most commonly observed. Switching between these domain types and various other domain configurations is interpreted, and the role of crystal imperfections in pinning the domain boundaries is discussed.

## 1. Introduction

Some perovskite-structured oxides exhibit ferroelectric behaviour and of these lead zirconium titanate (PZT) is now one of the best known. Minor additions of other metallic oxides modify and can improve its electrical properties. The perovskite-structured oxides PZT [1] and PLZT [2, 3] (where L represents lanthanum) can have either cubic, tetragonal, orthorhombic or rhombohedral symmetry depending on the temperature and their precise composition.

The modified-PZT ceramic that we have investigated by TEM techniques was developed by Whatmore and co-workers [4, 5] and has found applications in infrared detectors on account of its excellent pyroelectric properties. The ceramic has a chemical composition corresponding to $Pb(Fe_{0.20}Nb_{0.20}Zr_{0.58}Ti_{0.02})_{0.995}U_{0.005}O_3$ and it is ferroelectric at room temperature. Its symmetry is cubic above the transition temperature, 228° C, but as it is cooled below this temperature the cations are displaced in the $\langle 1\,1\,1\rangle$ directions from their cubic positions to give a rhombohedral unit cell. Associated with this distortion, an electric dipole is generated which is orientated along the rhombohedral axis. The elastic strain which accompanies the transition to the rhombohedral phase is equilibrated in bulk material by the formation of dipolar domains which relate to each other through a twin-like operation. In the ferroelectric phase there exists a structural phase transition which is associated with a tilting of the octahedral cage of oxygen ions, as described by Glazer [6, 7].

TEM studies of domains in oxide ferroelectrics have mainly been concerned with the tetragonal phases, e.g. $BaTiO_3$ [8], PZT [9] and $PbTiO_3$ [10] and there has been very little published on perovskite ferroelectrics in the rhombohedral phase.

## 2. Materials and experimental methods

Hot-pressed ceramics were made from high-purity oxide powders. Excess lead oxide, PbO, was added to starting materials to compensate for a tendency for PbO-deficiency to develop during fabrication and thus to obtain stoichiometry and also to form a liquid as an aid to densification. Grain sizes varied from 2 to 12 $\mu$m depending upon the temperatures and times used in the hot-pressing process and also upon the concentrations of PbO. Slices were cut from the hot-pressed blocks with a diamond saw and these were lapped down to a thickness of approximately 30 $\mu$m. They were then mounted on copper TEM grids and samples for TEM investigations were prepared by ion-beam thinning using 5 kV argon ions at an incidence angle of 12°. These low accelerating voltages and low ion currents were used to prevent loss of PbO and in order not to modify domain configurations. Observations were made with a JEOL 200CX microscope operated at 200 kV and also with a AEI EM7 microscope which could be fitted with both heating and liquid-nitrogen cooled specimen stages and was operated at a voltage of 1 MV.

## 3. A brief review of the application of TEM to the study of ferroelectric domains

Ferroelectric domains whose dipoles are related by twin-like operations cause splitting of electron diffraction spots in a direction in reciprocal space which is perpendicular to the domain walls, as first noted in $BaTiO_3$ [8]. The dynamical contrast of domain walls that are inclined to the electron beam is in accord with the properties of $\delta$-fringes on account of the dipole orientations giving different excitation vectors, $s_1$ and $s_2$, on either side of a domain wall. The nature of the extreme fringes in bright field (BF) and dark field (DF) can be used to determine the orientations of dipoles across a boundary as described by Gevers *et al.* [11, 12].

The symmetry of the structure is lowered in the paraelectric-to-ferroelectric transition because the dipole which appears in the unit cell as a result of

0022–2461/87 $03.00 + .12 

the displacement of the cations results in a non-centrosymmetric unit cell. Non-centrosymmetric crystals have specific effects on the dynamical diffraction contrast so that ferroelectric domain configurations (e.g. head-to-tail, head-to-head, or tail-to-tail dipole arrangements) can be inferred from the DF images obtained by using electron reflections corresponding to diffraction vectors perpendicular and parallel to the domain walls, as described by Gevers *et al.* [13].

Inversion boundaries (or 180° boundaries) exhibit characteristics which can also be explained in terms of the non-centrosymmetric properties of the crystal structure of the host material. When 180° boundaries are inclined to the electron beam they show $\alpha$-fringe diffraction contrast as described by Tanaka [14]. Other properties of inversion boundaries include the absence of any splitting of the diffraction spots when the field (diffraction) aperture is placed across an inversion boundary.

## 4. Observations

An example of the microstructure of the ceramic is shown in the low magnification micrograph, Fig. 1. Domains within the grains are seen to traverse them and to pin to the grain boundaries. The microstructure within grains can vary though the volume of a hot-pressed block, as also can the size of the grains. Intergranular glassy phases have been found to be spread inhomogeneously through the blocks, such glassy phases occurring mainly at triple grain junctions. Fig. 2 shows an example of a mainly glassy phase at a triple boundary junction. Micrograins can exist within the glassy phase. These micrograins have been observed to contain ferroelectric domains and have similar transition temperatures to the major grains. The micrograins have also been found to have internal microporosity – no microporosity is found in the larger grains.

The good pyroelectric properties of the modified PZT perovskite cause the ferroelectric domains to be quite mobile and unstable under the influence of the electron beam. Detailed analysis of the domains, which are commonly wedge-shaped, shows that the main twinning plane is $\{1\,1\,0\}$. These wedge-shaped domains are often periodic, with a periodicity of about 0.5 $\mu$m in the larger grains ($\sim 10\,\mu$m diameter). The domain walls themselves have been determined to range from 7 to 10 nm in thickness. These $\{1\,1\,0\}$-type domains have a head-to-tail dipole coupling and they are sometimes referred to as 109° domains. The non-centrosymmetric crystal properties cause invisibility when imaging with reflecting planes that are parallel to the wall, and this suggests that the displacement vector $\boldsymbol{R}$ of the twin-like operation is parallel to the wall. DF imaging of reflecting planes perpendicular to the wall gives strong differences in diffraction contrast between the adjacent domains. Fig. 3a illustrates this point and shows the light and dark contrast between periodic domains in the modified PZT. The selected-area diffraction pattern from the same region reveals small splittings in the high order diffraction spots (e.g. 6 3 3, inset and enlarged). This splitting is in a direction, [0 1 1], perpendicular to the domain wall. Twin domains on $\{1\,0\,0\}$, otherwise called 71° domains, are found more rarely than the $\{1\,1\,0\}$ domains. When these domains are inclined in the foil then $\delta$-fringes are seen, as in Fig. 4.

Closely-packed "strips" of domain are also frequently observed in the modified PZT and we shall refer to these as fine lamellar domains. The diffraction properties of this type of domain are similar to those of the head-to-tail wedge domains. These fine lamellar domains are sometimes found within wedge domains as illustrated in Fig. 5. The fine lamellar domains are thought to be of higher energy than the wedge domains because they often thermally switch to the latter after a short time under the electron beam.

One of the more interesting domain configurations found within the modified PZT has a domain wall which is highly-mobile when exposed to electron irradiation and has a zigzag character. The electron beam


*Figure 1* An example of the polycrystalline microstructure of modified hot-pressed PZT. Ferroelectric domains traverse the central grain from one grain boundary to another. BF micrograph.


*Figure 2* A region of glassy phase, containing a micrograin, situated at a triple junction in the ceramic. BF micrograph.

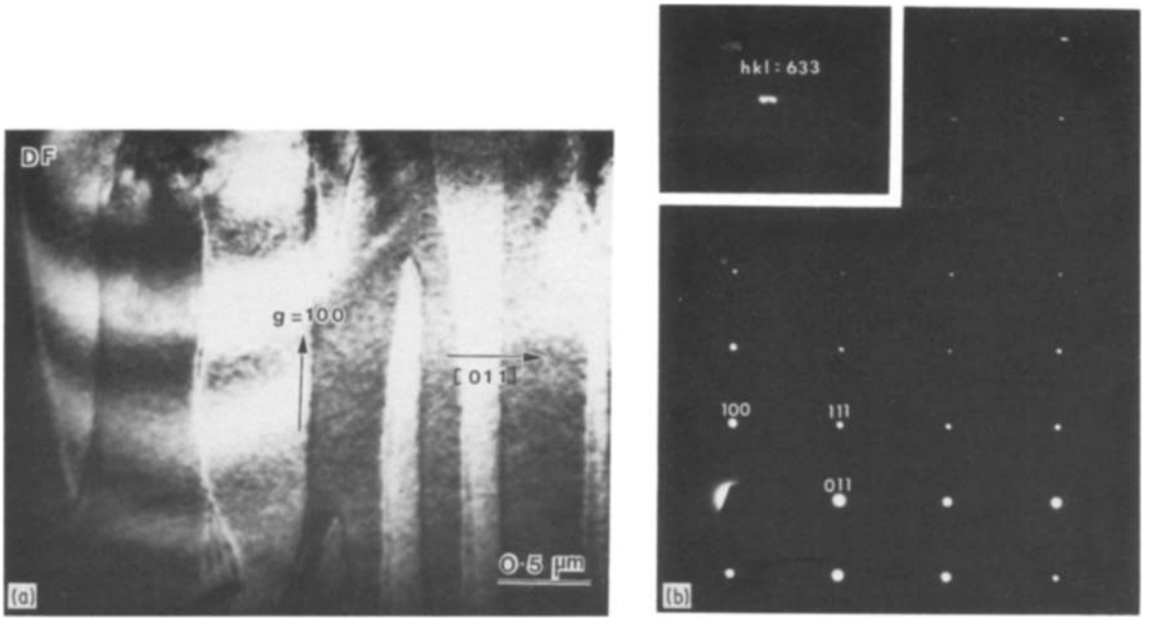


*Figure 3* (a) DF image of periodic domains imaged with the main diffraction vector parallel to the domain wall, (0 1 1). (b) Selected-area diffraction pattern from the periodic domains. Splitting of the diffraction spots is visible for high-order reflections, e.g. 6 3 3 (inset).

heating often induces expansion of the wall and this change stabilises the domains. Extensive migration of particular sections of the wall leads to the formation of the periodic wedge domains. Observations made on poled ceramic samples (i.e. those which have been subjected to an electric field at a high temperature) show that the first domain contrast to appear during thermal depoling is mostly associated with these zigzag boundaries. Figs 6a and b show two examples of zigzag head-to-head type domain boundaries. Because the serrations of the wall shown in Fig. 6b are coarser than those of the wall in Fig. 6a, the former are less mobile under the effect of the electron beam. A head-to-head boundary which is further developing the periodic wedge domains is seen in Figs. 7a and b. The elongations of the zigzag boundary leads to the formation of domains which are twinned on {1 0 0} planes. We note that at positions like X in the BF image there are discontinuities in the domain wall. In such regions the wall is invisible because there is a twin relationship across the wall with $\boldsymbol{R}$ perpendicular to $\boldsymbol{g} = 0\,1\,1$, but a head-to-head dipole arrangement is still present.

Domain mobility is often inhibited by microstructural barriers: we have already seen in Fig. 1 that domain walls may be pinned by grain boundaries. Another source of pinning is dislocations, as indicated by Fig. 8. In this modified PZT ceramic, the dislocations have predominantly screw-character and the slip-system is $\{1\,1\,0\}\ \langle 1\,\bar{1}\,0\rangle$, as has been found with other perovskite-structured systems [15, 16]. The local

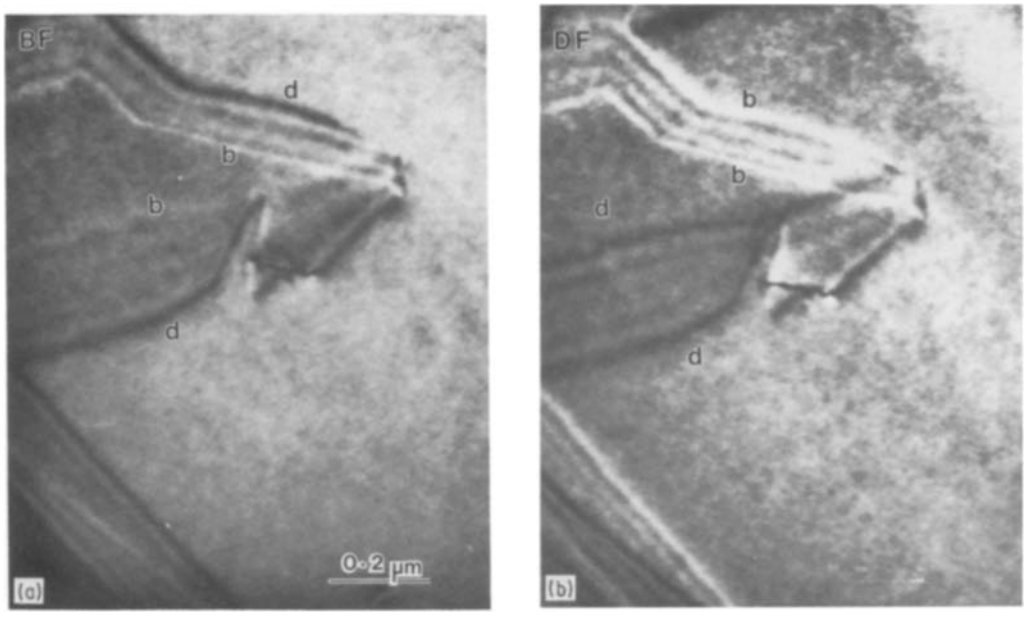


*Figure 4* (a) BF image of an inclined ferroelectric domain wall in modified-PZT: extreme fringes (indicated by b (bright) and d (dark)) are asymmetric. (b) DF image of the domain wall shown in (a): the extreme fringes, indicated by b and d, are now symmetric and hence have the characteristics of $\delta$-fringes.

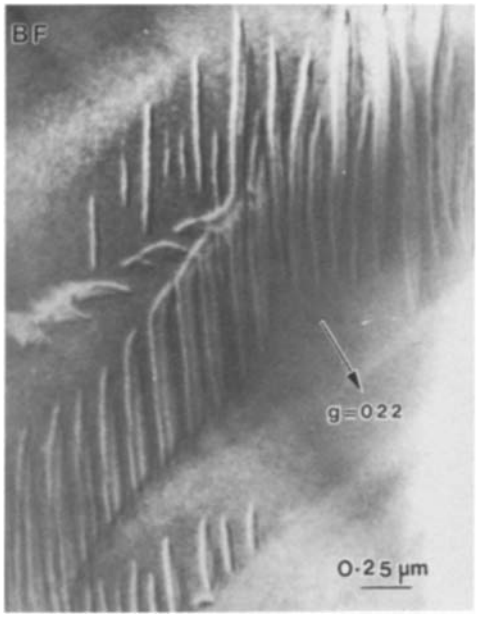


*Figure 5* BF image showing fine lamellar domains. These are pinned to a wedge domain, but it is invisible under the diffraction condition used (since $\boldsymbol{g} = 0\,2\,2$ is perpendicular to the domain wall).

elastic strain field of a dislocation acts as a nucleation site for the ferroelectric domains as specimens are cooled from the paraelectric to the ferroelectric phase. Also domains have the property of pinning each other and this can lead to complex domain configurations being built up throughout grains. A typical example is shown in Figs. 9a and b, in which the two BF images of the same field correspond to different diffraction conditions. Domains which are twinned on both $(0\,\bar{1}\,1)$ and $(1\,0\,0)$ are interacting. Inclined $(0\,0\,1)$ and $(\bar{1}\,1\,0)$ domain walls both have asymmetric fringes in these BF images. An inversion boundary (180° domain wall) is seen which corresponds to a $(\bar{2}\,1\,\bar{1})$ plane and this boundary has symmetrical fringes.

## 5. Discussion

The behaviour of the wedge-like domains is very similar to that of 90° domain walls in ferroelectrics with tetragonal symmetry, like $BaTiO_3$ and $PbTiO_3$. The domain wall thickness and the periodicity in the modified PZT are of a similar order to those in the above tetragonal materials. Selected-area diffraction patterns of PZT show a splitting of the diffraction spots, but the splitting is not as great as for $BaTiO_3$ and $PbTiO_3$ samples at room temperature. This is an indication that the distortion of the ferroelectric cell in the rhombohedral PZT is not as great as in the tetragonal phases and hence the microscopic dipole polarization is also smaller. In the case of the rhombohedral symmetry (where a cubic cell can distort in any of the four $\langle 1\,1\,1\rangle$ directions) head-to-tail twinning can, in principle, occur on $\{1\,1\,0\}$ or $\{1\,0\,0\}$ planes, but we mainly observe it on the $\{1\,1\,0\}$ planes. A Landau-type calculation based on the work of Zhirnov [17] (see Appendix) reveals that in the rhombohedral system a twin boundary on the $\{1\,1\,0\}$ plane has a surface energy, $\sigma$, that is only one-third of that of a twin boundary on a $\{1\,0\,0\}$ plane. If we assume that the number of twins on a particular plane is determined by the Maxwell–Boltzmann distribution (namely $\propto \exp(-E_i/k_B T)$ where $E_i$ is energy, $k_B$ is Boltzmann's constant and $T$ the absolute temperature) then

$$\frac{\text{Number of } \{1\,0\,0\} \text{ domains}}{\text{Number of } \{1\,1\,0\} \text{ domains}} \approx \frac{\exp(-3\sigma)}{\exp(-\sigma)} \approx 0.14$$

In agreement with this theory, $\{1\,1\,0\}$ domains are observed to occur more frequently than the higher energy $\{1\,0\,0\}$ type.

The Zhirnov calculation suggests that a component of polarization, $P$, parallel to the domain wall will vary according to the hyperbolic expression $P = P_0 \tanh(x/\delta)$ across a domain wall of thickness $\delta$, where $x$ is the coordinate in a direction perpendicular to the wall. Thus on approaching the centre of the domain wall the dipole vanishes and its strength increases in magnitude with distance from the wall on the other side. This differs from the ferromagnetic system where the dipole rotates across the domain wall and does not vanish at any position.

In the case of domain configurations, the dipole arrangement attempts to reduce the energy of the

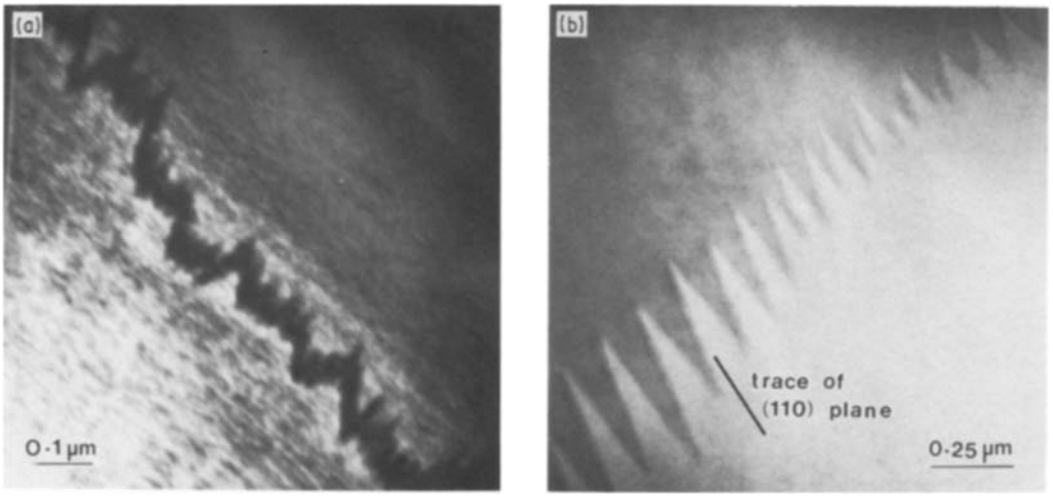


*Figure 6* (a) BF micrograph showing a head-to-head (or tail-to-tail) domain arrangement with a fine-scale zigzagging domain boundary. (b) BF micrograph showing head-to-head domains at the stage where they are beginning to stabilize by the coarsening of the zigzag domain boundary.

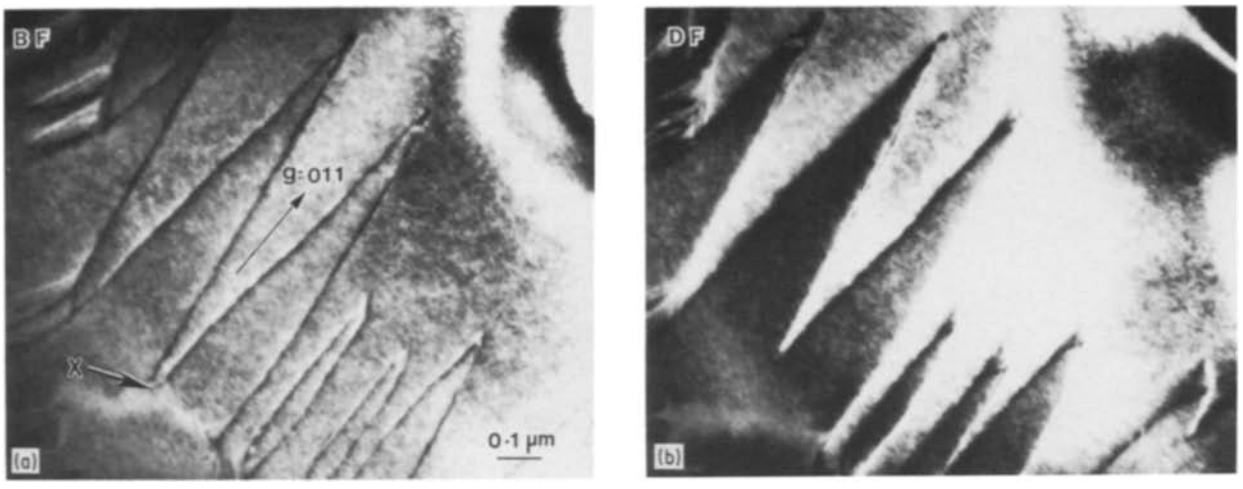


*Figure 7* (a) BF image of the domain boundary walls between head-to-tail domains which have formed from head-to-head domains. (b) DF image corresponding to (a) obtained with a diffraction vector which is parallel to the head-to-tail- and perpendicular to the head-to-head-dipole walls.

non-uniform distribution of the polarization in the transition region, i.e. div $\boldsymbol{P}$ must be reduced. The zigzag domains described in an earlier section are similar to those described by Yakunin *et al.* [18] in tetragonal $BaTiO_3$. Yakunin *et al.* have suggested that these domains have a head-to-head dipole configuration, with the zigzags acting as a source of microscopic head-to-tail coupling in order to reduce the electrostatic self-energy. Observations of the thermal switching to the periodic wedge domains in the modified-PZT also suggest that this is the situation. Fig. 10 demonstrates how this switching takes place.

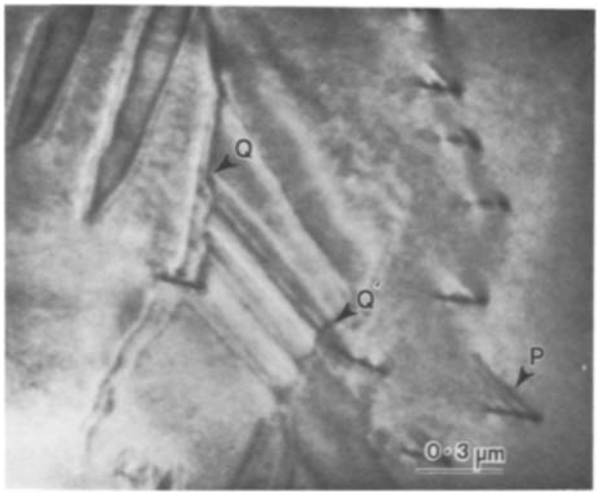


*Figure 8* BF micrograph showing two types of domain wall interaction. At P a domain wall is pinned to a dislocation and at Q, Q′ domains are pinned between two domain walls.

By using the non-centrosymmetric properties of a rhombohedral ferroelectric we can distinguish between the two types of domain configuration. Fig. 11a is a diagram of the head-to-tail configuration across a $\{1\,1\,0\}$ wall. The dipole is shown resolved into components parallel and perpendicular to the domain wall. Comparing the components, we can see that the non-equivalent (i.e. $\{1\,0\,0\}$) planes are perpendicular to the domain wall. DF imaging of these planes gives strong diffraction contrast.

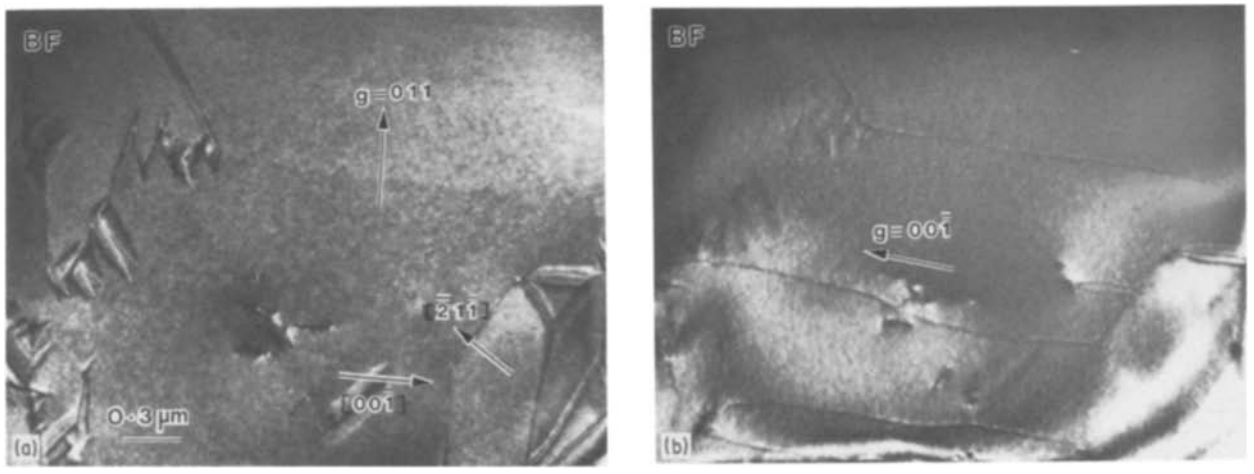


*Figure 9* (a, b) Two BF micrographs, obtained with different reflections, showing that complex domain configurations exist within the grains of hot-pressed ceramic.

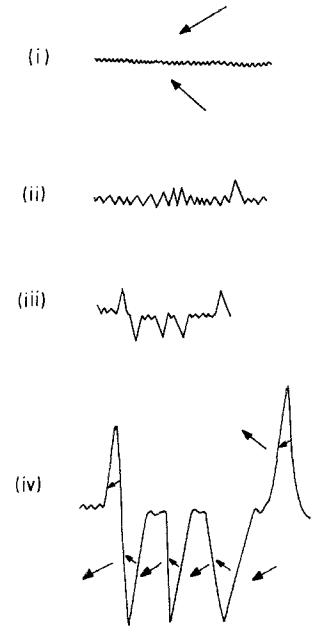


*Figure 10* Schematic diagram to illustrate the thermal switching of a head-to-head domain arrangement to the periodic head-to-tail form.

Fig. 11b is a diagram of the head-to-head configuration across a {1 0 0} wall. In this case the non-equivalent {1 0 0} planes are parallel to the domain wall plane, and thus DF imaging using these reflecting planes gives strong diffraction contrast in accordance with non-centrosymmetric behaviour.

The highly mobile head-to-head domains may well be of great importance to the pyroelectric properties of the modified PZT. Since we observe these domains to be in the majority as grains depole in the electron microscope, such domains may be very important in normal thermal-depoling.

The TEM study has revealed factors which may reduce the efficiency of achieving optimum pyroelectric properties of these ceramics. These include the intergranular glassy phases which reduce the proportion of thermally-sensitive material in a given volume of detector. Domain pinning by microstructural defects will also give rise to dielectric loss, since domain mobility will be inhibited, so that dislocation densities must be kept to a minimum. Fortunately in the material that we have examined, the densities of dislocations are low.

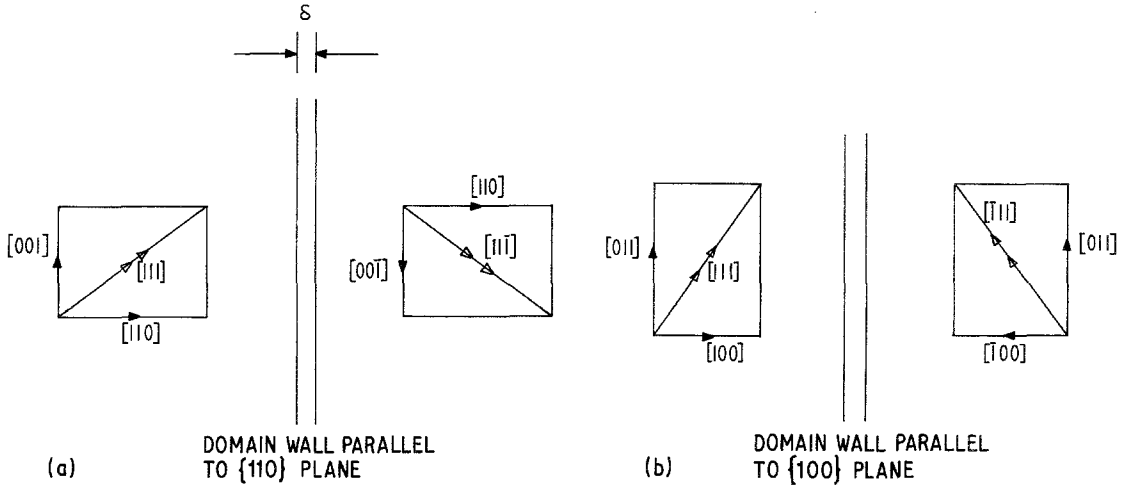


*Figure 11* Diagrams showing the non-equivalent components of dipolar distortion in (a) head-to-tail and (b) head-to-head domains.

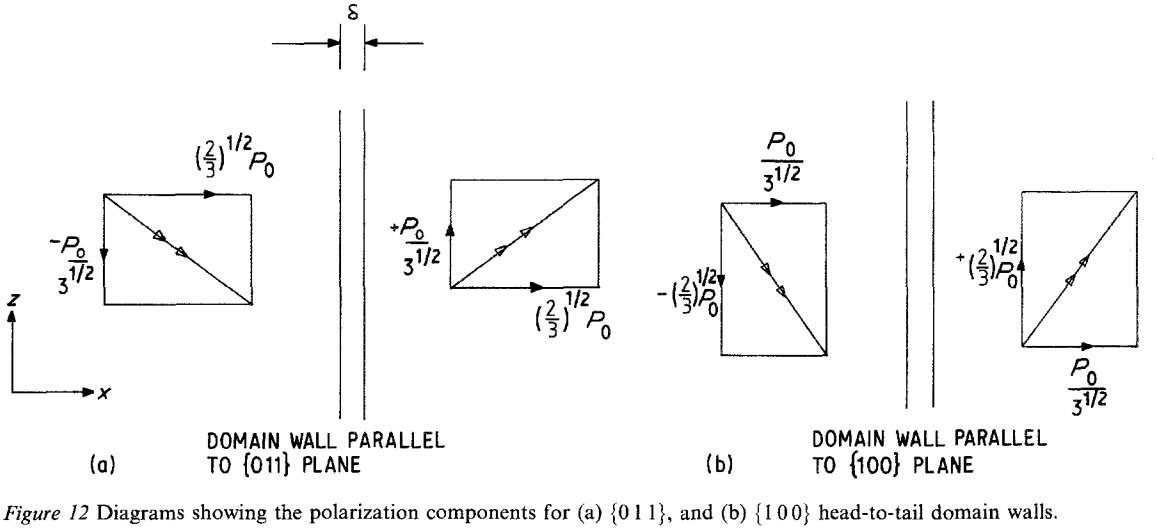


*Figure 12* Diagrams showing the polarization components for (a) {0 1 1}, and (b) {1 0 0} head-to-tail domain walls.

## Appendix

If we adopt a generalized free energy $\phi$ for a domain with the dipole lying in a plane, following the calculations of Zhirnov [17], we obtain

$$\phi = \phi_0 + \frac{\chi}{2}[(\nabla P_y)^2 + (\nabla P_z)^2] + \frac{a}{2}P_y^2 + \frac{b}{2}P_z^2 + \frac{c_1}{4}P_y^4 + \frac{c_2}{4}P_z^4 + \frac{d_1}{2}P_y^2P_z^2 \quad \text{(A1)}$$

where $(\chi/2)(\nabla \boldsymbol{P})^2$ is an exchange energy. The coefficients of the polarization terms are complex expressions of tensors which include electrostriction, elastic constants and deformations. For the case of rhombohedral symmetry we take a dipole to lie in a plane such that the polarization can be expressed as a vector $\boldsymbol{P} = P_0[(2/3)^{1/2}, (1/3)^{1/2}]$ within this plane.

We now can consider the dipoles on either side of both $\{0\,1\,1\}$ and $\{1\,0\,0\}$ twin walls.

Referring to Figs 12a and b, we have resolved the polarization of the dipoles into components parallel and perpendicular to the domain wall for both possible twin planes. These components are considered at positions far away from the domain wall region (or transition region). The domain wall has a width, $\delta$. To find the conditions for the minimum energy when the domains are in thermodynamic equilibrium we apply Euler–Lagrange equations to Equation (A1) and thus find that

$$\chi P_y'' = a_1P_y + c_1P_y^3 + d_1P_y^2P_z^2$$
$$\chi P_z'' = b_1P_z + c_2P_z^3 + d_1P_z^2P_y^2 \quad \text{(A2)}$$

We then apply the following boundary conditions to the $\{1\,0\,0\}$ domains:

$$\text{at } x = -\infty, \quad P_x = -(2/3)^{1/2}P_0,$$
$$P_y = 0 \quad \text{and} \quad P_z = P_0/3^{1/2}$$

and obtain solutions of minimum energy:

$$P_z = -\frac{P_0}{3^{1/2}}\tanh\frac{x}{\delta_1}$$

where

$$P_0 = \frac{3b}{c_2} \quad \text{and} \quad \delta_1 = \left(\frac{6\chi}{c_2}\right)^{1/2}P_0^{-1} \quad \text{(A3)}$$

$\delta_1$ is the width of the transition region across the domain wall. The excess surface energy of a $\{1\,1\,0\}$ domain wall is

$$\sigma_{\{1\,1\,0\}} = \int_{-\infty}^{\infty}(\phi - \phi_{00})\,dx = \frac{4}{9}\left(\frac{2\chi}{3}c_2\right)^{1/2}P_0^3 \quad \text{(A4)}$$

where $\phi_{00}$ is a free energy expression corresponding to the situation when no domain wall is present.

We can similarly find expressions for the $\{1\,0\,0\}$–71° domain wall. In this case the excess surface energy is found to be

$$\sigma_{\{1\,0\,0\}} = \frac{4}{9}\left[\chi c_2\left(\frac{16}{3}\right)\right]^{1/2}P_0^3 \approx 3\sigma_{\{1\,1\,0\}}$$


## Acknowledgements

The work was made possible through research grant GR/C/29072 and a CASE studentship (C.A.R.) sponsored by the Allen Clark Research Centre (Caswell), both awarded by the Science and Engineering Research Council. We gratefully acknowledge access to the 1 MV EM7 electron microscope at the Imperial College of Science and Technology, London, and the technical assistance of Mr J. Woodall of Imperial College. We also thank Dr D. R. Tilley for his help with the Landau calculation and also Mr T. Goodwin for his valuable technical assistance, both of the University of Essex.


## References


1. B. JAFFE, W. R. COOK and H. JAFFE, "Piezoelectric Ceramics" (Academic Press, London, 1971) p. 136.
2. E. T. KEVE and K. L. BYE, *J. Appl. Phys.* **46** (1975) 810.
3. H. M. O'BRYAN and A. H. MEITLZER, in Proceedings of Conference on Phase Transitions and their Applications to Materials Science, edited by H. K. Henish, R. Roy and L. E. Cross (Pergamon Press, New York, 1973).
4. R. W. WHATMORE, J. M. HERBERT and E. W. AINGER, *Phys. Status Solidi (a)* **61** (1980) 73.
5. R. W. WHATMORE and A. J. BELL, *Ferroelectrics* **35** (1981) 155.
6. A. M. GLAZER, *Acta Cryst.* **B28** (1972) 3384.
7. *Idem, ibid.* **A31** (1975) 756.
8. M. TANAKA and G. HONJO, *J. Phys. Soc. Jpn* **19** (1964) 954.
9. E. K. GOO, R. K. MISHRA and G. THOMAS, *J. Appl. Phys.* **52** (1981) 2940.
10. A. A. DOBRIKOV and O. V. PRESNYAKOV, *Kristall Tech.* **15** (1980) 1317.
11. R. GEVERS, P. DELAVIGNETTE, H. BLANK and S. AMELINCKX. *Phys. Status Solidi* **4** (1964) 383.
12. *Idem, ibid.* **5** (1964) 595.
13. R. GEVERS, H. BLANK and S. AMELINCKX, *ibid.* **13** (1966) 449.
14. M. TANAKA, in Proceedings of Eighth International Conference on Electron Microscopy, Canberra, 1974, Vol. 1, edited by J. V. Sanders and D. J. Goodchild (Australian Acad. Sci. Canberra, A.C.T., Australia, 1974) p. 556.
15. C. A. RANDALL, D. J. BARBER and R. W. WHATMORE, Institute of Physics Conference Series No. 78, Proc. EMAG '85, Newcastle upon-Tyne (Institute of Physics, London, 1985) p. 531.
16. V. V. PRISEDSKY, G. F. PAN'KO and V. V. KLIMOV, *Ferroelectrics* **64** (1985) 257.
17. V. A. ZHIRNOV, *Sov. Phys. JETP* **35** (8) (1959) 822.
18. S. I. YAKUNIN, V. V. SHAKMANOV, G. V. SPIVAK and N. V. VASIL'EVA, *Sov. Phys. Solid State* **14** (1972) 310.
19. M. E. LINES and A. M. GLASS, "Principles and Applications of Ferroelectrics and Related Material" (Clarendon Press, Oxford, 1977).



*Received 21 April*
*and accepted 30 June 1986*